Available online at www.sciencedirect.com
SCIENCE DIRECT®
International Journal of Heat and Mass Transfer 48 (2005) 3294–3307
International Journal of HEAT and MASS TRANSFER
www.elsevier.com/locate/ijhmt

# Effects of thermal spot configurations on the flow through porous media driven by natural and forced convection

R.A. Bortolozzi, J.A. Deiber *

*Instituto de Desarrollo Tecnológico para la Industria Química, INTEC (UNL-CONICET), Güemes 3450-S3000 GLN Santa Fe, Argentina*

Received 12 August 2004; received in revised form 25 February 2005

**Abstract**

A study concerning the flow of a Newtonian fluid through a porous medium for the particular case natural convection is produced by hot and cold spots placed in the solid phase is presented. Results involving the interaction of forced convection with thermal spots are reported to visualize the mechanisms associated with the generation of complex flow patterns in the porous medium. For this purpose the computation of a two-field model is carried out. Two systems are studied: one is a rectangular porous cavity (RPC) of square cross section and the other is an annular porous cavity (APC) comprised by two concentric vertical cylindrical walls. It is shown, in general, that the flow patterns associated with each configuration and intensities of the thermal spots may be qualitatively inferred by following rules that are established through a basic study of mixed convection in the RPC.


*Keywords:* Natural convection; Mixed convection; Thermal spots; Porous media; Two-field model

## 1. Introduction

At present, the evaluation of the velocity field and the heat flux, both generated by natural and forced convection in a porous medium containing cold and hot spots of variable intensity, is a relevant subject of practical interest. Multiple technological applications in different industrial equipments and electronic devices require the detailed knowledge of velocity and temperature fields under this particular situation. For instance, it has been reported that the quality of grain and cereal storage and drying in silos is affected by the generation of hot spots in the granular bed, which are caused by fungal growth and grain germination, among other naturally occurring phenomena [1,2]. Also, flow maldistributions may induce hot spots in packed-bed reactors as a consequence of destabilization of the basic uniform flow typically assumed in designs; thus, the effective conversion of reactants may be quite different from the nominal value expected, usually with an inhomogeneous product due to undesired side reactions [3,4]. In similar systems, strongly localized stationary and traveling hot spots arise when changes in gas velocity occur in the catalytic combustion of hydrogen in monolith reactors [5]. Another challenging problem involves thermal control by appropriate air cooling of integrated circuits, which are at present configured under significant miniaturization and reduction of spaces between them [6,7]. Thus,

* Corresponding author. Tel.: +54 342 4559175; fax: +54 342 4550944.
*E-mail address:* treoflu@ceride.gov.ar (J.A. Deiber).

0017-9310/$ - see front matter © 2005 Elsevier Ltd. All rights reserved.
doi:10.1016/j.ijheatmasstransfer.2005.02.025

**Nomenclature**

| | |
|---|---|
| $a$ | thermal dispersion coefficient |
| $a_v$ | specific surface of porous medium, $m^{-1}$ |
| $b$ | Forchheimer inertial constant, m |
| $C_f^0$ | fluid heat capacity at constant pressure, J/kg K |
| $d_p$ | particle diameter, m |
| $D$ | width of porous cavity, m |
| $Da$ | Darcy number ($=K_\infty/D^2$) |
| $Fs$ | Forchheimer number ($=b_\infty/D$) |
| $\boldsymbol{g}$ | gravity acceleration, $m/s^2$ |
| $G_0$ | dimensionless source or sink intensity ($=S_0D^2/\Delta T k_{m\infty}$) |
| $Gr$ | Grashoff number ($=(\rho_f^0)^2 g\beta K_\infty D\Delta T/(\mu_f^0)^2$) |
| $h_f$ | fluid heat-transfer coefficient, $W/m^2$ K |
| $h_s$ | solid heat-transfer coefficient, $W/m^2$ K |
| $h_{sf}$ | solid–fluid heat-transfer coefficient, $W/m^2$ K |
| $H$ | Sparrow number ($=h_{sf}D^2a_v/k_{m\infty}$) |
| $\boldsymbol{I}$ | unity tensor |
| $k_\alpha$ | thermal conductivity, W/m K ($\alpha$ = s, f) |
| $k_m$ | stagnant thermal conductivity of the saturated porous medium, W/m K |
| $\boldsymbol{k}_d^*$ | dimensionless thermal dispersion tensor |
| $K$ | permeability of the porous medium, $m^2$ |
| $l_c$ | characteristic length for heat transfer in the solid phase, m |
| $L$ | height of the porous cavity, m |
| $Pe$ | Peclet number ($=U_\infty D/\alpha_f^0$) |
| $Pr_f$ | fluid Prandtl number ($=C_f^0\mu_f^0/k_f^0$) |
| $Q_h$ | dimensionless heat flux at the hot wall, defined by Eq. (7) |
| $Q_c$ | dimensionless heat flux at the cold wall, defined by Eq. (8) |
| $r_i$ | inner radius of porous cavity, m |
| $r_o$ | outer radius of porous cavity, m |
| $r_v$ | ($=\boldsymbol{V}/\widehat{\boldsymbol{V}}$) |
| $Ra$ | Rayleigh number ($=\rho_f^0 g\beta K_\infty D\Delta T/\mu_f^0\alpha_{m\infty}$) |
| $Ra_f$ | fluid Rayleigh number ($=Ra/Da\lambda$) |
| $Re_p$ | particle Reynolds number ($=\rho_f^0\varepsilon\lvert\boldsymbol{v}_f\rvert d_p/\mu_f^0$) |
| $S_0$ | source or sink intensity of thermal spot, $W/m^3$ |
| $T_\alpha$ | temperature, K ($\alpha$ = s, f) |
| $T_i$ | wall temperature, K ($i$ = h, c) |
| $U_\infty$ | maximum superficial velocity at the cavity entry, m/s |
| $\boldsymbol{v}_f$ | fluid velocity, m/s |
| $\boldsymbol{V}$ | dimensionless superficial velocity for natural convection |
| $\widehat{\boldsymbol{V}}$ | dimensionless superficial velocity for forced convection |
| $x$ | horizontal coordinate, m |
| $X$ | ($=x/D$) |
| $z$ | vertical coordinate, m |
| $Z$ | ($=z/D$) |

*Greek symbols*

| | |
|---|---|
| $\alpha_{m\infty}$ | thermal diffusivity of saturated porous medium ($=k_{m\infty}/\rho_f^0C_f^0$), $m^2/s$ |
| $\beta$ | isobaric thermal expansion coefficient, $K^{-1}$ |
| $\gamma$ | ($=d_p/D$) |
| $\varepsilon$ | porous medium porosity |
| $\Theta_\alpha$ | dimensionless temperature ($\alpha$ = s, f) |
| $\kappa$ | ($=r_o/r_i$) |
| $\lambda$ | ($=k_f^0/k_{m\infty}$) |
| $\mu_f^0$ | fluid viscosity, Pa s |
| $\nu$ | ($=k_s^0/k_{m\infty}$) |
| $\rho_f^0$ | fluid density, $kg/m^3$ ($\alpha$ = s, f) |
| $\sigma$ | heat dispersion around the peak |
| $\Psi$ | streamline |

*Subscripts*

| | |
|---|---|
| c | cold wall |
| f | fluid phase |
| h | hot wall |
| m | properties of composite (solid and fluid) |
| s | solid phase |
| w | wall |
| $\infty$ | any property far from cavity walls |

*Superscript*

| | |
|---|---|
| 0 | property of pure species |

since the circuit densities are significantly increased with inevitable higher power dissipation, the internal offset fin structures may be modeled as a saturated non-isothermal porous medium [8]. Therefore, for design purposes, heat transfer limitations must be appropriately evaluated in relation to the relative position of hot and cold spots. In this sense, although natural convection can be used as a mean of thermal control providing a vibration-free environment in contraposition to forced convection [9], one observes that flow paths are rather complex around thermal spots, affecting thus the intensity of heat transfer and placing the need to seek for the optimal cooling configuration.

In a wider context of practical situations, rather different from that described above, it is also clear that natural and mixed convections of a fluid saturating a porous medium has received much attention in the literature at present [10,11] mainly without the inclusion of heat sources; those including thermal spots are significantly a few less [2,12–14]. In particular, the presence

of hot and cold spots in the porous medium places relatively new problems to be considered and solved. In fact, typically these thermal spots are generated in only one of the two phases involved (the fluid or the solid) or alternatively it can be the results of a complex mechanism involving heat generation and heat transfer at the solid–fluid interface. As mentioned above, there are many practical situations where the heat source is placed in the solid particles and heat emanates from them. It is precisely in this type of systems where the use of two-field porous media models becomes important for design purposes because the assumption of local thermal equilibrium is not valid [12,15].

The two-field model (2-F model) for a rigid porous matrix studied previously [16] is used here to avoid the condition of local thermal equilibrium usually valid for other situations already analyzed in the literature (see, for example, [17]). It is shown here that the intensity of the two types of thermal spots significantly control the heat transfer problem in the configurations proposed in this study. Also we evaluate the flow patterns under different configurations of thermal spots to obtain a rationale of flow movement and control. With these purposes, two cavities are studied: (1) rectangular porous cavity (RPC) of square cross section with a very large axial length perpendicular to the gravity vector [Fig. 1(a)] and (2) annular porous cavity (APC) comprised by two vertical concentric cylindrical walls [Fig. 1(b)]. In both cases, when natural convection is considered, the upper and lower walls are adiabatic and the lateral walls (inner and outer walls for the APC) are kept at constant temperatures, which may have either the same or different values. When mixed convection (natural and forced) is considered, the temperature of fluid entering to the cavity is assumed uniform and the temperature at the exit of the cavity approaches its final value asymptotically along the axial coordinate.

In relation to the arrangements of thermal spots in the cavities, one observes that there is a high number of configurations possible, increasing it with the number of spots. Therefore, for the purposes of this study we choose different configurations of four spots. Of course, a larger number of spots greater than four is prone to be analyzed through periodically placed boundary conditions as observed in Section 3.

The outline of this work is as follows: first, we present briefly the 2-F model including thermal spots and boundary conditions. Then, this model is applied to the RPC and APC with different configurations of four thermal spots, where natural and mixed convections may be present. After the analysis and discussion of the main numerical results, rules allowing one to infer qualitatively the flow patterns in the porous cavity due to the thermal spots are established.

## 2. Theoretical analysis

The 2-F model [15,18,19] uses the balance equations of momentum and energy to study natural and mixed convections in a porous medium saturated with a Newtonian fluid. This model considers the Darcy–Brinkman–Forchheimer terms for the steady-state movement of the fluid phase and includes a variable porosity near the wall containing the porous medium. Also, the model considers dispersion phenomena due to fluid convective fluctuations in the interstices of the solid matrix, which are assumed isotropic. Since the energy balance is required for both solid and fluid phases, an exchange of heat between phases is included [12].

### 2.1. Balance equations

Following previous works for natural convection [16,20] here a more general version of the resulting dimensionless model is presented, which may be used to study both natural and mixed convection problems with thermal spots in the RPC and APC considered above. Therefore, the dimensionless mass balance is,

$$\nabla \cdot \widehat{\boldsymbol{V}} = 0 \tag{1}$$

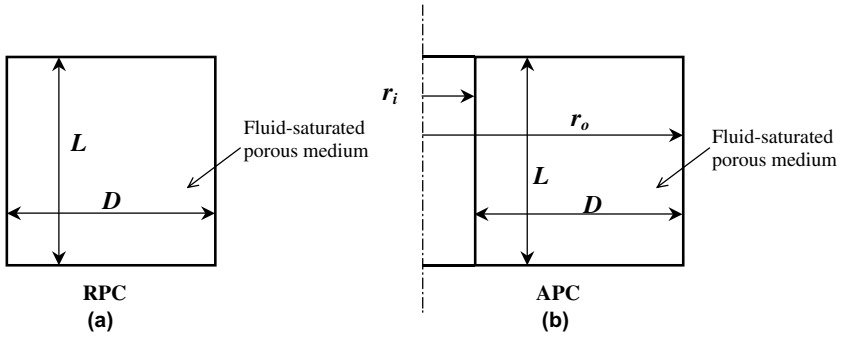


Fig. 1. Scheme of porous medium cavities: (a) rectangular porous cavity (RPC), (b) annular porous cavity (APC).

The dimensionless momentum of the fluid phase is expressed

$$\frac{Da\,Pe}{\varepsilon Pr_f}\widehat{\boldsymbol{V}}\cdot\nabla\widehat{\boldsymbol{V}} = \frac{Gr\,Pr_f}{Pe}\varepsilon\Theta_f\boldsymbol{k} - \frac{\varepsilon}{\phi_1}\left(1+\phi_2 Fs\frac{Pe}{Pr_f}|\widehat{\boldsymbol{V}}|\right)\widehat{\boldsymbol{V}} + Da\nabla^2\widehat{\boldsymbol{V}} \tag{2}$$

and two dimensionless energy balances must be formulated; thus,

$$\lambda Pe\,\widehat{\boldsymbol{V}}\cdot\nabla\Theta_f = \nabla\cdot[(\lambda\varepsilon\boldsymbol{I}+\boldsymbol{k}_d^*)\cdot\nabla\Theta_f] - H(\Theta_f-\Theta_s) \tag{3}$$

pertains to the fluid, and

$$\nabla\cdot[v(1-\varepsilon)f_c\nabla\Theta_s] + H(\Theta_f-\Theta_s) + \sum_{i=1}^{n} G_i = 0 \tag{4}$$

is satisfied by the solid phase, where $n$ thermal sources and sinks are included through $G_i$. In Eqs. (1)–(4), dimensionless numbers are appropriately defined to describe mixed convection consistently with previous works. Also, for a closed cavity, where the fluid is moving by natural convection only, the characteristic velocity used is $\alpha_{m\infty}/D$.

The two energy balances are expressed through the dimensionless temperatures of the fluid $\Theta_f = \frac{T_f - T_c}{\Delta T}$ and the solid $\Theta_s = \frac{T_s - T_c}{\Delta T}$, where $\Delta T = T_h - T_c$. Here $T_h$ and $T_c$ are used to designate the temperature of hot and cold cavity walls, respectively. For the cases in which both vertical walls of the RPC and APC cavities are at the same temperature, $\Delta T$ is defined as the difference between $T_{max}$ and $T_w$; where $T_{max}$ is the higher temperature within the porous cavity and $T_w$ is the wall temperature. For cold spots (heat sinks) $\Delta T$ is defined, however, with the $T_{min}$ counterpart. In addition, in Eq. (2) the dimensionless functions $\phi_1 = \frac{K(\varepsilon)}{K_\infty}$ and $\phi_2 = \frac{b(\varepsilon)}{b_\infty}$ tend to one far away from the cavity walls.

The dimensionless numbers in Eqs. (1)–(4) and those used to describe natural convection in a previous work [20] are related through the following simple expressions: $r_v = Pe\lambda$ and $Ra = Gr\,Pr_f\,\lambda$. When $\widehat{\boldsymbol{V}}$ and these relations are introduced into Eqs. (1)–(4), the dimensionless model for natural convection is consistently obtained [16].

In the balance equations, $\varepsilon$ is the porosity that varies near the cavity walls according to $\varepsilon = \varepsilon_\infty[1 + A\exp(-\frac{Bn}{d_p})]$ [21], where $A$ and $B$ are constants and $n$ is the normal distance from any wall. The 2-F model involves the stagnant thermal conductivity of the mixture $k_m = k_f + k_s$ as defined in [20] and [22]. Also, in the energy balances [Eqs. (3) and (4)] of the fluid and solid phases, $H$ is the Sparrow number [12], where $h_f$ is obtained from previous works [20,23] and $h_s = k_s^0/l_c$ includes a characteristic porous medium length $l_c$ that is of the order of $d_p/10$ for spheres [24]. In Eq. (3), the dimensionless dispersion tensor $\boldsymbol{k}_d^* = \gamma l a|\boldsymbol{V}|\boldsymbol{I}$ is defined according to Mercer et al. [25], where $l$ is the Van Driest function [26].

In this work thermal spots are simulated through Gaussian functions placed as thermal sources and sinks in the energy balance of the solid phase [Eq. (4)]. Therefore each thermal spot in the porous medium may be described through the following dimensionless expression (subscript $i$ is omitted):

$$G(X,Z) = \frac{G_0}{2\pi\sigma^2}\exp\left\{-\frac{1}{2}\left(\frac{X-X_0}{\sigma}\right)^2\right\} \times \exp\left\{-\frac{1}{2}\left(\frac{Z-Z_0}{\sigma}\right)^2\right\} \tag{5}$$

where $X_0$ and $Z_0$ are the dimensionless coordinates of the center, $G_0$ is the thermal spot intensity and $\sigma$ is the heat dispersion around the peak thermal intensity.

It is worth to mention that several authors used a modified Rayleigh number that included the heat source [2,14]. In this work a dimensionless number in the source term of the solid energy balance expressed $G_0 = \frac{S_0 D^2}{\Delta T k_{m\infty}}$ is defined, which resulted similar to that defined by Alex et al. [13]. Here $S_0$ is the dimensional source (or sink) intensity of the thermal spot. Also, $G_0$ multiplied by the Rayleigh number is proportional to the dimensionless number used by Jiménez-Islas et al. [2] and Kim et al. [14].

In previous works, point sources were considered as a good approximation to an intensity $G_0$ distributed in a finite domain of the solid matrix [12], and several studies involved an uniform heat generation in a packed bed [2,13,14]. Other interesting works have placed the heat sources at the walls of the porous cavity [9,27].

### 2.2. Boundary conditions

When natural convection is present in the porous cavities only, the non-slip velocity condition implies $\widehat{\boldsymbol{V}} = \boldsymbol{0}$ at vertical and horizontal walls. The temperature fields must satisfy the adiabatic condition at horizontal walls ($Z = 0$ and 1) through $\frac{\partial\Theta_f}{\partial Z} = 0$, and $\frac{\partial\Theta_s}{\partial Z} = 0$, while $\Theta_f = \Theta_s = 1$ for the hot wall ($X = 0$), and $\Theta_f = \Theta_s = 0$ for the cold wall ($X = 1$). On the other hand, $\Theta_f = \Theta_s = 0$ is considered for the particular case the vertical walls are at the same temperature $T_w$, consistently with the temperature normalization discussed above.

For the case of mixed convection considered in the RPC only, the upper and lower boundary conditions of the cavity must be modified. In fact, the velocity field entering the porous cavity has the following expression:

$$\widehat{V}_z = \frac{\cosh\left[\sqrt{\frac{\varepsilon}{Da}}\left(X-\frac{1}{2}\right)\right] - \cosh\left[\frac{1}{2}\sqrt{\frac{\varepsilon}{Da}}\right]}{1-\cosh\left[\frac{1}{2}\sqrt{\frac{\varepsilon}{Da}}\right]} \tag{6}$$

which is again recovered asymptotically at the exit of the cavity. This expression is obtained by solving the one-directional problem, when the porosity variation near the vertical walls at the inlet is neglected (see, for example, [28]) and the Forchheimer number is considered very small. This is an appropriate and simple approximation for the purposes of placing more realistic boundary conditions. The velocity field at vertical walls (non-slip) is the same as the case of pure natural convection, but the temperature field is required to satisfy $\Theta_f = \Theta_s = 0$ at $Z = 0$ (entrance) and $\frac{\partial^2 \Theta_f}{\partial Z^2} = 0$ and $\frac{\partial^2 \Theta_s}{\partial Z^2} = 0$ at $Z = 1$ (exit) while the vertical walls are kept at constant temperature giving $\Theta_f = \Theta_s = 0$.

The resulting model [Eqs. (1)–(4)] is expressed in finite differences and solved numerically by following the procedure described in our previous work [20].

## 3. Results and discussion

Following our previous comments in the introduction section, we present relevant numerical results concerning several configurations of hot and cold spots in the RPC and APC. This discussion is carried out in two sections. In Section 3.1, only cases of natural convection are considered, while in Section 3.2 cases associated with mixed convection are analyzed, which are indeed useful to understand the previous ones. In fact, natural convection has a characteristic velocity defined indirectly through thermo-physical properties and, of course, it may not be controlled in a direct manner. In this section, we describe phenomena in detail and their physical explanations are then proposed.

### 3.1. Natural convection

#### 3.1.1. One thermal spot in the RPC with vertical walls at different temperatures

With the purpose of characterizing the flow and heat transfer phenomena that occur in a porous medium with thermal sources and sinks, first we consider the case where one thermal spot is placed at the center of the RPC while the vertical walls are at different temperatures. A basic flow is obtained when there is not any thermal spot in the cavity and the fluid movement is the result of natural convection induced by the temperature difference of the vertical walls (see, for instance, [29]). Therefore, when a hot spot is placed at the cavity center, a substantial distortion of streamlines in relation to those of the basic flow is observed. Since the system is in steady-state, the heat entering and leaving the RPC is exactly balanced with the heat exchanged through the thermal spots inside the cavity. The heat fluxes at the hot $Q_h$ and cold $Q_c$ vertical walls in dimensionless form, are:

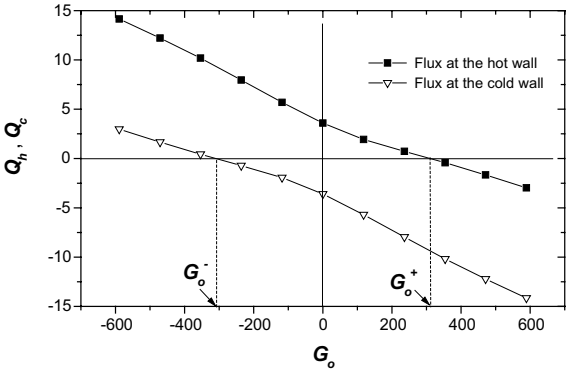


Fig. 2. Heat fluxes of hot and cold walls as function of the intensity of thermal spot ($G_0 > 0$ for source and $G_0 < 0$ for sink). Parameters are: $Ra_f = 1.36 \times 10^8$, $Da = 10^{-5}$, $Pr_f = 4.60$, $L/D = 1$, $\lambda = 0.747$, $\varepsilon_\infty = 0.40$, $A = 0.30$, $B = 7.5$, $\gamma = 0.1$ and $a = 0.1$.

$$Q_h = \frac{q_h D}{k_{m\infty}\Delta T} = -\int_0^1 \left(\lambda\varepsilon\frac{\partial\theta_f}{\partial X} + v(1-\varepsilon)f_c\frac{\partial\theta_s}{\partial X}\right)dZ \quad \text{at } X = 0 \tag{7}$$

$$Q_c = \frac{q_c D}{k_{m\infty}\Delta T} = \int_0^1 \left(\lambda\varepsilon\frac{\partial\theta_f}{\partial X} + v(1-\varepsilon)f_c\frac{\partial\theta_s}{\partial X}\right)dZ \quad \text{at } X = 1 \tag{8}$$

Eqs. (7) and (8) are defined with the convention that the heat flux is positive when thermal energy is entering the cavity, while a negative value indicates the opposite. Fig. 2 shows $Q_h$ and $Q_c$ as a function of the intensity of thermal spot $G_0$. When $G_0$ is negative, a heat sink exists in the porous cavity and the heat leaving the cold wall is less than that entering through the hot wall. The opposite is true when $G_0 > 0$. In particular when the intensity of the thermal spot is significant, critical values $G_0^+$ and $G_0^-$ are found where an inversion of the heat flux sign in one of the vertical walls is expected. One also concludes that $Q_h = -Q_c$ when sources and sinks are not present in the porous cavity only.

The above discussion concerning the macroscopic heat balance in the RPC is also relevant to prove at each numerical run the consistence of the computational code generated in this work. In fact, the difference between the heat leaving and entering the RPC shall be equal to the heat exchanged through the thermal spot with intensity $G_0$, which is obtained by integrating $G(X, Z)$ within the whole volume of the porous cavity.

#### 3.1.2. One thermal spot in the RPC with vertical walls at the same temperature

In this case, the fluid movement is induced by the presence of one thermal spot (source or sink of heat)

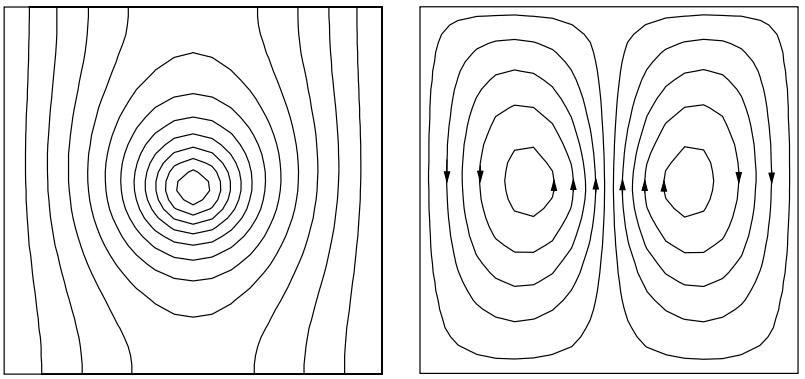


Fig. 3. (a) Solid phase isotherms ($0 \leqslant \Theta_s \leqslant 1$) and (b) streamlines ($-1.20 \leqslant \Psi \leqslant 1.20$) for RPC with a hot spot at the center. Parameters are the same as in Fig. 2. The hot spot intensity is $G_0 = 188.80$. Spot heat dispersion is $\sigma = 2.2$.

in the porous cavity. In this sense, Fig. 3(a) shows a hot spot placed at the center of the RPC. The solid-phase isotherms forming a sharp thermal gradient at the RPC center are concentric with the hot spot. There exists also a critical temperature below which the isotherms become symmetrically open up. Temperatures of the solid phase are higher than $T_w = T_h = T_c$. Fig. 3(b) shows that the streamlines for this case present two symmetric vortices; the right one is rotating clockwise while the left one is counterclockwise. The vortex centers are placed slightly above the horizontal central plane of the cavity.

When a heat sink is in place of the heat source, the vertically inverted pictures (180° rotation) of isotherms and streamlines are obtained. Therefore, this situation presents vortex rotations that are the opposite of those corresponding to the hot spot (not shown here). Further, in this case the temperatures in the solid phase are less than $T_w$, and the vortex centers are placed a little below the horizontal central plane of the cavity.

Before ending this section, it is appropriate to discuss briefly the effect of parameters $Da, \gamma = d_p/D$ and $L/D$ on numerical solutions, having into account that other dimensionless numbers pertain to typical systems composed by water and glass or ceramic beads. For this purpose, one thermal spot in the RPC with vertical walls at the same temperature is considered. Numerical results show the following: (a) when $Da$ is increased from $10^{-5}$ to $10^{-2}$, the fluid velocity passing through the hot spot is also increased. Therefore inertial effects push the centers of the two vortices upward and the fluid moves faster near the vertical walls generating very sharp momentum and thermal boundary layers (this effect is also observed, for instance, in Figs. 5 and 7); (b) when $\gamma$ takes values from 0.01 to 0.2 the effect on thermal and flow patterns are similar to those found for increments of Darcy number; (c) when $L/D$ is changed from 0.5 to 1.5 one observes that the number of vortices are the same as in the squared cavity and the flow patterns accommodate conformably to the new aspect ratio of the porous cavity.

### 3.1.3. Several thermal spots in the RPC with vertical walls at the same temperature

Here we are concerned with the presence of several thermal spots in the RPC and the possibility of controlling the flow direction through the variation of places and intensities of cold and hot spots. The vertical walls are at the same temperature, and the horizontal walls are adiabatic. As elementary cell for the flow domain, four thermal spots are studied in the porous matrix, the center of which are placed at the following coordinates values $(X, Z)$: $(L/4, D/4)$, $(L/4, 3D/4)$, $(3L/4, D/4)$ and $(3L/4, 3D/4)$. Fig. 4 presents a scheme of the five configurations selected as being relevant to illustrate basic phenomena associated with the heat transfer problem, which of course, pertains to a high number of possibilities that cannot be all analyzed in this work. These configurations are numbered from 1 to 5 and discussed below.

*3.1.3.1. Configuration 1.* Four hot spots (heat sources) of the same intensity are considered. Fig. 5(a) shows the isotherms of the solid phase. In the cavity zone, where the two upper spots are placed, the temperature values are relatively high indicating a local heating due to the presence of the upper adiabatic wall. The two lower spots generate a similar effect but the temperatures in this zone are lower than those of the upper one due to the colder fluid coming from below. In fact, this fluid was previously cooling along the isothermal vertical walls. Fig. 5(b) shows the corresponding streamlines where one observes the fluid rises through the hot

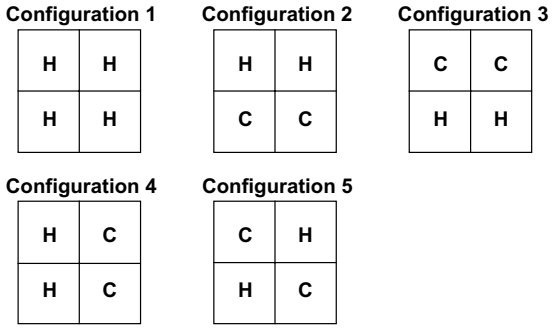


Fig. 4. Scheme showing the configurations of four thermal spots placed in the porous cavity analyzed in this work. Letters H and C refer to hot and cold spots, respectively. Thermal spots are placed at the center of each cell resulting from the division in four equal parts of the transversal section of the porous cavity.

spots and then fall down near the vertical walls at a temperature $T_w$. Thus in the porous medium two symmetric vortices are established, with opposite rotating direction as already described in Fig. 3(b) above.

When the same configuration of thermal spots is considered in the APC, the effect on the flow patterns of the radial variation of annular concentric areas is introduced. It is thus observed that the APC modifies substantially the isotherms and the streamlines in relation to those corresponding to the RPC. The symmetry of thermal and flow patterns is lost due to the APC geometry. Therefore, an intensive vortex flow is established on the right hand side of the APC [Fig. 5(d)], which is interacting directly with the four hot spots, while the left vortex is of a rather weak intensity, and it is driven mainly by the two left hot spots placed in the APC.

*3.1.3.2. Configuration 2.* In this case the hot spots are placed in the upper half space of the cavity while the cold spots are below them (Fig. 4). The four spots have the same absolute value of intensity (signs are negative for sinks and positive for sources). The temperature field

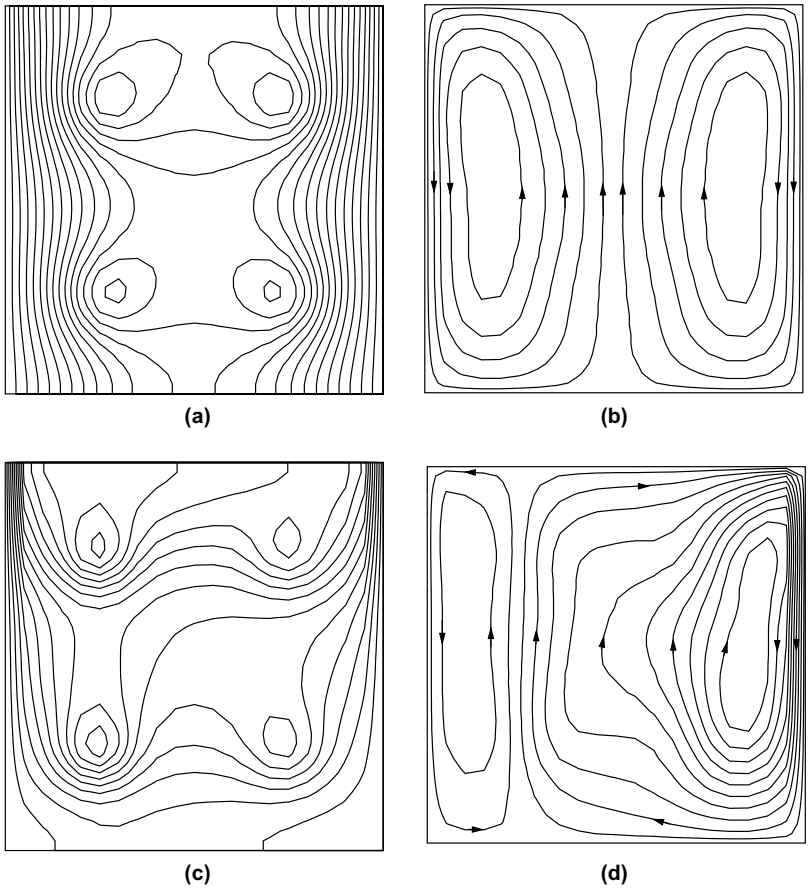


Fig. 5. Numerical solutions for Configuration 1 (Fig. 4) with four hot spots of equal intensity: (a) solid phase isotherms ($0 \leqslant \Theta_s \leqslant 1$) and (b) streamlines ($-1 \leqslant \Psi \leqslant 1$) for RPC; (c) solid phase isotherms ($0 \leqslant \Theta_s \leqslant 1$) and (d) streamlines ($-0.3 \leqslant \Psi \leqslant 1.4$) for APC. Also, $G_0 = 47.20$ and $\sigma = 2.20$. Other parameters are the same as in Fig. 2. For APC, $\kappa = 5.338$.

thus obtained is depicted in Fig. 6(a). The streamlines are presented in Fig. 6(b), where one observes the presence of four vortices. In the upper part, the fluid recirculates counterclockwise at the left, and the opposite at the right. In addition the fluid moves upward mainly through the hot spots and the central zones of the cavity, then moves downward from outside of the hot spots and near the vertical walls. From the middle plane downward the opposite fluid behavior is found. Thus a stagnation point is formed at the center of the cavity [see Fig. 6(b)] generating a pure stretching deformation.

This thermal spot configuration is also analyzed in the APC [Fig. 6(c) and (d)] and once more the symmetry of thermal and flow patterns of the RPC are lost due to geometry. When one compares these results with those of Fig. 5(c) and (d), the differences found are significant; in fact, on the right hand side of the APC two intensive vortices are found interacting with the four thermal spots. Two other vortices of rather weak intensity are placed on the left, which are driven by the left thermal spots.

*3.1.3.3. Configuration 3.* Two cold spots are in the upper part of the cavity and two hot spots are below (Fig. 4). In addition two different situations are analyzed: one considers that the absolute values of the four intensities are equal (even intensities) and the other involves hot spots with a higher absolute value of the heat intensity than that of the cold spots (uneven intensities). For even intensities [see isotherms in Fig. 7(a)] the fluid is moving in the cavity similarly to Configuration 2, but the direction of rotation of the four vortices are exactly the opposite [compare Fig. 6(b) and Fig. 7(b)]. The relevant changes are found, however, with the situation involving uneven intensities [Fig. 7(c) and (d)]. Thus, starting from the center of the lower part of the cavity [Fig. 7(d)], the hot spots yield a significant upward flow that collides with the cold spots and channels toward the

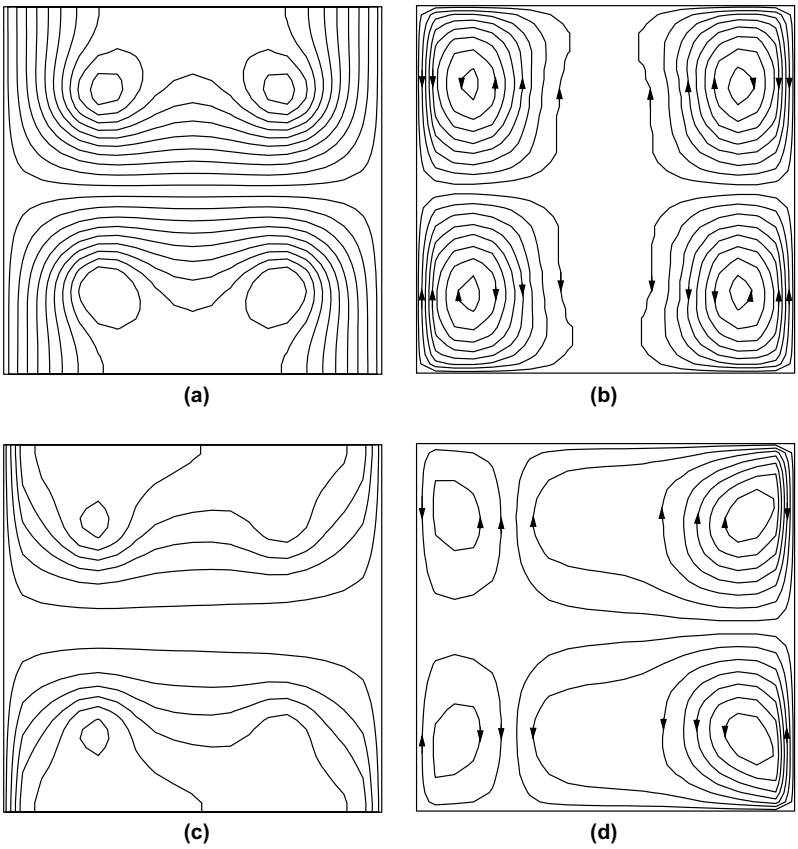


Fig. 6. Numerical solutions for Configuration 2 (Fig. 4) with two hot spots and two cold spots: (a) solid phase isotherms ($-0.8 \leqslant \Theta_s \leqslant 1$) and (b) streamlines ($-0.50 \leqslant \Psi \leqslant 0.50$) for RPC; (c) solid phase isotherms ($-0.9 \leqslant \Theta_s \leqslant 1$) and (d) streamlines ($-0.55 \leqslant \Psi \leqslant 0.55$) for APC. Spot intensities are: $G_0 = 47.20$ (hot spots or sources) and $G_0 = -47.20$ (cold spots or sinks). Other parameters are the same as in Fig. 2. For APC, $\kappa = 5.338$.

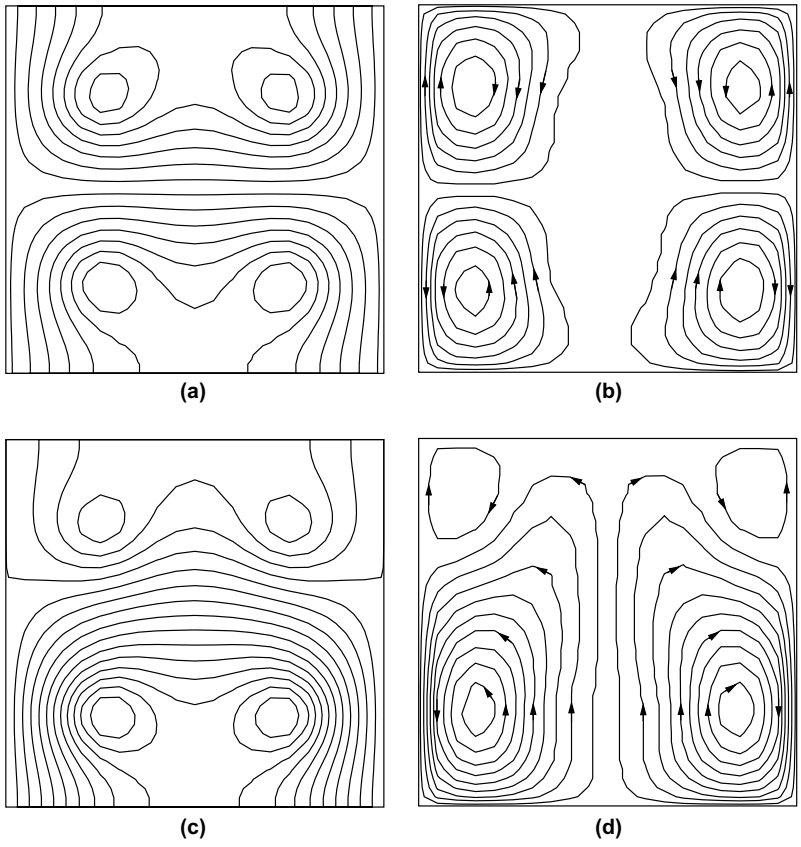


Fig. 7. Numerical solutions for Configuration 3 (Fig. 4) with two cold spots and two hot spots in the RPC: (a) solid phase isotherms ($-0.9 \leqslant \Theta_s \leqslant 1$); (b) streamlines ($-0.45 \leqslant \Psi \leqslant 0.45$) for $G_0 = 47.20$ (sources) and $G_0 = -47.20$ (sinks); (c) solid phase isotherms ($-0.3 \leqslant \Theta_s \leqslant 1$) and (d) streamlines ($-0.60 \leqslant \Psi \leqslant 0.60$) for $G_0 = 47.20$ (sources) and $G_0 = -23.60$ (sinks). Other parameters are the same as in Fig. 2.

cavity center. Then, the top adiabatic wall stops the fluid, which must fall down obliquely through the cold spots. When leaving the cold spots, the fluid is repelled by the hot spots turning toward the vertical walls and falling down with a sharp momentum boundary layer along them [see details in Fig. 7(d)], to reach then the lower adiabatic wall where the circulation loop reinitiates. The hot-spot-recirculation zones confining the other part of fluid are significantly larger than those corresponding to the cold spots. From this configuration, it is clear that one may form very subtle fluid trajectories in a porous medium by combining different configurations and intensities of thermal spots.

*3.1.3.4. Configuration 4.* In this particular case, the two hot spots are on the left and two cold spots are on the right of the RPC (Fig. 4). Fig. 8(a) shows that the heat propagates upwards from the hot regions while this situation is inverted around the cold spots. The resulting flow is observed in Fig. 8(b) where a big vortex is formed almost occupying the whole RPC. The ascending part of this vortex moves through the hot spots while the descending portion of the fluid moves through the cold spots. In addition, the vortex is complemented with two weak vortices diagonally opposed, which are rotating in the counterclockwise direction. For this particular situation the moment boundary layers observed on the vertical wall of the previous cases are not any more present as a consequence of the dumping effect introduced by the diagonally opposed small vortices. It should be pointed out that this thermal configuration does not give symmetric thermal and flow patterns, despite the study is carried out in the RPC.

*3.1.3.5. Configuration 5.* Before the discussion of some important results from the previous sections, we consider Configuration 5 presented in Fig. 4, where cold and hot spots are placed diagonally opposed, respectively, in the RPC. The four spots have the same absolute value of thermal intensity. Fig. 9(a) shows that the

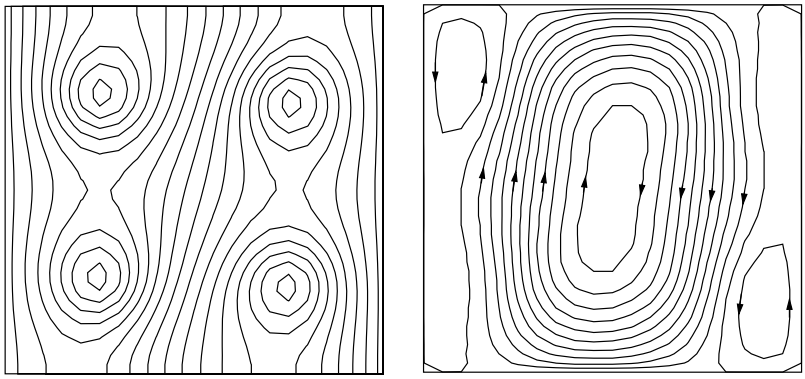


Fig. 8. (a) Solid phase isotherms ($-1 \leqslant \Theta_s \leqslant 1$) and (b) streamlines ($-0.20 \leqslant \Psi \leqslant 1.20$) for RPC with two hot spots and two cold spots (Configuration 4—Fig. 4). Spot intensities are: $G_0 = 47.20$ (sources) and $G_0 = -47.20$ (sinks). Other parameters are the same as in Fig. 2.

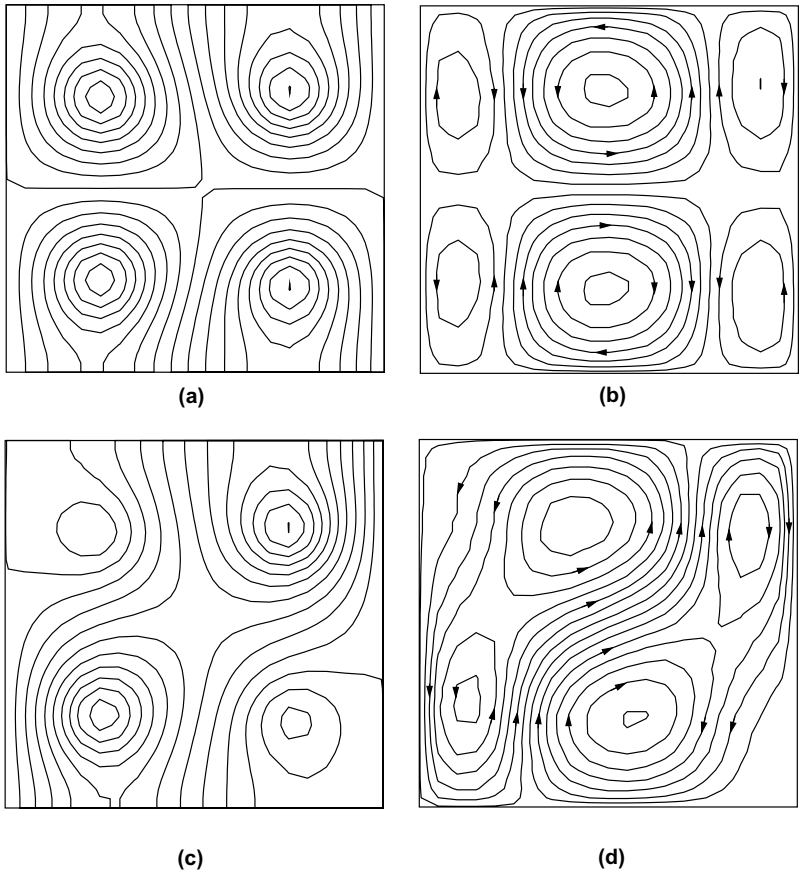


Fig. 9. Numerical solutions for Configuration 5 (Fig. 4) with two cold spots and two hot spots in RPC: (a) solid phase isotherms ($-0.8 \leqslant \Theta_s \leqslant 1$); (b) streamlines ($-0.6 \leqslant \Psi \leqslant 0.6$) for $G_0 = 47.20$ (sources) and $G_0 = -47.20$ (sinks); (c) solid phase isotherms ($-0.3 \leqslant \Theta_s \leqslant 1$) and (d) streamlines ($-0.45 \leqslant \Psi \leqslant 0.50$) for $G_0 = 47.20$ (sources) and $G_0 = -23.60$ (sinks). Other parameters are the same as in Fig. 2.

RPC has four zones involving isothermal lines. These thermal zones yield, however, six vortices [Fig. 9(b)] where the circulating directions are alternated (the upper left vortex is clockwise). There are two big central vortices and four lateral weak vortices in the RPC. When the configuration involves the same location of thermal spots, but the hot spots have a higher intensity than that of the cold spots, a zone of high temperature is observed covering the diagonal of the RPC from lower left corner to upper right corner [see Fig. 9(c)]. Interesting is the fact that the fluid is channeling through this high temperature zone [Fig. 9(d)] diagonally from left to right to turn back looking for the cold spots. The six vortices of the previous configuration are reduced now to four vortices and a high interaction between thermal spots is present. Despite the flow patterns of Fig. 9(b) and (d) belong to the same thermal configuration, one finds that the corresponding flow fields are significantly different from one another due to the effect of the thermal spots intensities. The opposite case (increasing the intensity of cold spots) yields a similar situation (not presented here) but the diagonal for fluid channeling is perpendicular to that one of the case already discussed.

It is clear here that the natural convection flow patterns generated by hot and cold spots either in the RPC and the APC may be quite complex mainly depending on the configuration of the thermal spots and their intensities. In addition the number of combinations, and hence of phenomenological situations are very high and rather tedious to be analyzed one by one. In addition they are rather difficult to infer qualitatively from the physical point of view, at least some simple physical criteria are established to guide our intuition in order to be able to visualize these flow patterns without complex numerical calculations. These criteria of course will give us a tool for design purposes as pointed out in the introduction section. In this sense, we found that the way to visualize these criteria is to study numerically the mixed convection in the RPC. From these results, several practical rules in terms of fluid attractors and fluid repellers may be obtained by changing the intensity of the forced convection. Thus, when forced convection is absent, the natural convection system is recovered; on the other hand, by increasing substantially forced convection its naturally occurring counterpart is minimized. What is more important here is the fact that the fluid will move upward through hot spots and downward through cold spots independently from the type of the dominant convection, as it is visualized in the Section 3.2.

#### *3.1.4. Flow pattern similarities with other porous medium systems*

Before closing Section 3.1, it is interesting to point out that the flow patterns found in a porous cavity heated from below (see, for instance, [30], for the Bénard problem in porous media) are similar to those of a horizontal sequence of alternating hot and cold spots placed between the upper and lower adiabatic walls according to results reported in Figs. 8 and 9(a) and (b). To achieve this configuration one is naturally introducing a condition of periodicity on the lateral walls of the porous cavity. In addition, following to this result, one may be interested to place two layers with alternating hot and cold spots and observes that two cases emerge: (1) if the thermal spots of equal sign are placed one above the other, the results are the existence of long vortices involving each one four thermal spots (two cold and two hot) moving from the lower to the upper boundary through the hot spots and conversely through the cold spots. (2) If the thermal spots of different signs are placed one above the other, the streamlines follow the patterns proper of each layer (Bénard type) and the vortices are of course of the size allowed by each layer. Thus, the flow situation is similar to several Bénard layers one above the other with the vortices rotating as if they are placed in a ''gear box''. Finally, when one compares the situations involving a configuration with the periodicity analyzed above and that with the same configuration but with the lateral barriers placed (the lateral isothermal walls are now considered) the conclusion is that the flow patterns are quite the same except near the barriers where half of the vortices are observed due to their presence.

Another case where flow patterns are similar with the results of the present work is thermovibrational heat transfer [31]. In fact the temporal evolution of the vortices structure found for thermovibration in a rectangular porous enclosure may be compared to a steady-state sequence of different configurations of hot and cold spots. Thus, each time of the development of the thermovibrational phenomenon (Fig. 87, p. 149 of Ref. [31]) may be compared with Fig. 7(b) discussed above. In fact, a squared porous cavity subjected to thermovibration generates four vortices of the size of 1/4 of the cavity extend. Increasing the time, the number of vortices is reduced until only one vortex remains in the steady-state. This situation can be compared to configurations 3 and 4 of our Fig. 7(b) and Fig. 8(b). The flow pattern changes occurring in thermovibrational convection are associated with the evolution of the temperature fields in the solid matrix of the porous medium. In fact, at short times, when the fluid receive heat from below, the system response behaves as that represented in Fig. 7(b) with configuration 3, where two hot spots are below and two cold spots are above. For a later time, the fluid movement transfers heat to the upper part of the cavity, which yields a gradual change of the temperature field. This phenomenon generates the diagonal interaction of vortices: two vortices fuse into a bigger one and the two ones remaining are diminishing in size at the corner of the cavity until they disappear.

### 3.2. Mixed convection

As mentioned above, here we consider that fluid is entering in the RPC from below at a given flow rate [see Eq. (6)]. To achieve the purpose of this section and also to be brief enough, only two cases are analyzed: one has a hot spot placed at the center of the RPC, while the other involves instead a cold spot. In addition the flow rate is varied from zero (natural convection) to values for which forced convection is predominant.

#### 3.2.1. One hot spot in the RPC with vertical walls at the same temperature

This case is similar to that reported in Fig. 3. Nevertheless, when the flow rate is different from zero, one observes a decrease of the size of the two vortices present in the cavity and the appearance, of course, of open streamlines connecting the inlet and outlet of fluid in the cavity [Fig. 10(a)]. By increasing the flow rate even more, the vortex sizes become smaller and the fluid is significantly channeling through the cavity center [Fig. 10(b)]. One may say that the hot spot is an attractor of the fluid moving upward, against the gravity vector. At high flow rates the two vortices disappear and the streamlines become more parallel (sweeping off the effect of the hot spot) due to the intense convection [Fig. 10(c)]. Further, to obtain a situation similar to that shown in Fig. 10, for instance, the intensity of the heat spot must be increased by a factor of around twelve when $Pe$ is 10 times greater. Thus, the phenomenon manifestation depends mainly on the relative values between the magnitudes of Peclet number and intensity of thermal spot.

In relation to this part of our study it is appropriate to consider the work of Lai et al. [27], where the flow of a Newtonian fluid through a porous cavity with a thermal source in the lateral boundary is investigated. This zone of higher temperature than the rest of the porous cavity yields flow patterns similar to those found for a hot spot in Fig. 10, of course, as long as one takes into account the geometrical differences pertaining to each case. Thus the common result is that streamlines tend to get together around the hot zone due to the attraction of the fluid moving upward (see also point b in relation to Lai et al. work [27]).

#### 3.2.2. One cold spot in the RPC with vertical walls at the same temperature

In this case, when the flow rate is null, natural convection generates again two vortices that circulate in opposite directions with respect to the previous case of a hot spot. Thus fluid falls down through the cavity center and moves upward near the lateral walls, as it was already discussed in relation to Fig. 3. Once more, when fluid enters the cavity from below, the size of the symmetric vortices decreases and they are surrounded by open streamlines (Fig. 11). Nevertheless, a significant difference is observed in the flow patterns pertaining to the cold spot from those of the hot spot: the cold spot

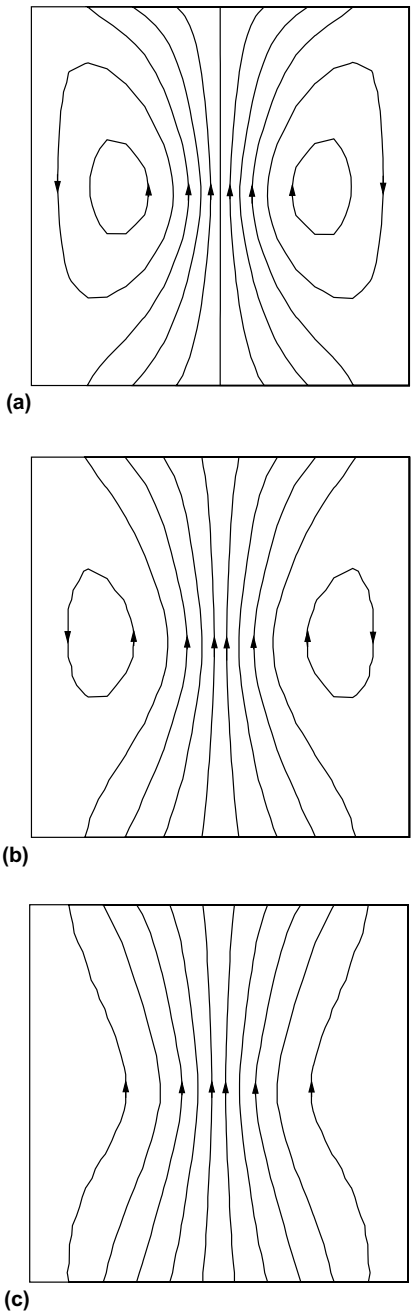


Fig. 10. Streamlines in RPC with a hot spot in the cavity center and fluid entering from below: (a) $Pe = 0.0134$ and $-0.50 \leqslant \Psi \leqslant 0.50$; (b) $Pe = 0.0335$ and $-1.25 \leqslant \Psi \leqslant 1.25$; (c) $Pe = 0.0670$ and $-2.40 \leqslant \Psi \leqslant 2.40$. Other parameters are: $Gr = 30$, $Da = 10^{-5}$, $Pr_f = 4.60$, $L/D = 1$, $\lambda = 0.747$, $\varepsilon = 0.40$, $\gamma = 0.1$, $a = 0.1$, $G_0 = 188.80$, $\sigma = 0.80$.

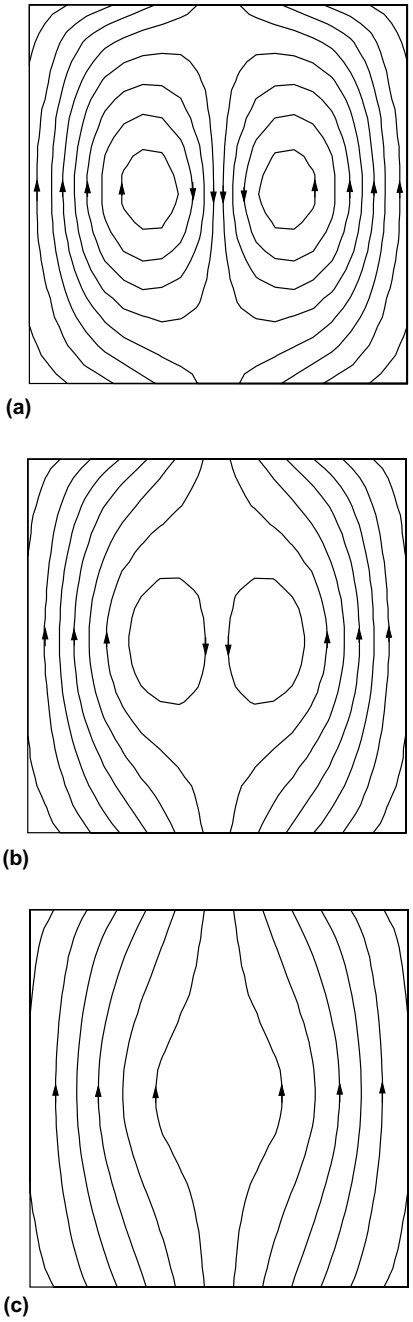


Fig. 11. Streamlines in RPC with a cold spot in the cavity center and fluid entering from below: (a) $Pe = 0.0134$ and $-0.50 \leqslant \Psi \leqslant 0.50$; (b) $Pe = 0.0335$ and $-1.25 \leqslant \Psi \leqslant 1.25$; (c) $Pe = 0.0670$ and $-2.50 \leqslant \Psi \leqslant 2.50$. Parameters are the same as in Fig. 10, except $G_0 = -188.80$.

is a repeller of the fluid moving upward (against the gravity vector) as clearly illustrated through Fig. 11. At high flow rates the two vortices tend to disappear once more [Fig. 11(c)] and the streamlines become more parallel (sweeping off the effect of the cold spot) due to the intense convection.

By considering the work of Lai et al. [27] again, where the flow patterns followed by the fluid entering the porous enclosure from above are shown (in the direction against to the gravity vector) but still in relation to a hot spot at the boundary, it is found yet a more interesting analogy with our results. In fact this situation is similar to the fluid repulsion of the cold spot of our Fig. 11. Thus, it is clear that this discussion reaffirms the results presented above in the sense that the four mixed convection problems related to one thermal spot and the flow direction with respect to the gravity vector can be resumed in only two basic problems, as it is described in our Section 4, points (a) and (b). They are: the repulsion and the attraction phenomena.

## 4. Conclusions

The present study provides the theoretical and phenomenological understanding of how the temperature and velocity fields are generated either by natural and mixed convections in the RPC and APC with thermal spots. The summary of conclusions that allows one to interpret isotherms and streamlines in the porous cavity are: (a) a hot spot is an attractor of the fluid moving upward (against the gravity vector) and repels the fluid moving downward. (b) A cold spot repels the fluid moving upward (against the gravity vector) and attracts the fluid moving downward. (c) Both effects apply to natural as well as to mixed convection. (d) The intensities of thermal spots (negative for cold spot or sink, and positive for hot spot or source), which can differ in absolute value from one type another, is controlling significantly the channeling and both thermal and momentum boundary layers of fluid throughout the porous cavity. Thermal intensities together with configurations of thermal spots control the fluid movement in the porous cavity. (e) Flow patterns in the RPC differ significantly from those of the APC for the same configuration and intensity of thermal spots. (f) There exist flow situations generated by different means (for instance, Bénard problem and thermovibrational heat transfer) which are similar to those given by configurations of thermal spots in the porous cavity.

## Acknowledgement

Authors wish to thank the financial aid received from Universidad Nacional del Litoral, Santa Fe, Argentina (CAI+D 2002), SEPCYT-FONCYT (PICT 09-09752) and CONICET (PIP 02554).

## References


[1] D. Brooker, F.W. Bakker-Arkema, C.W. Hall, The Drying and Storage of Grains and Oilseeds, Van Nostrand Reinhold, New York, 1992, pp. 378–379.

[2] H. Jiménez-Islas, F. López-Isunza, J.A. Ochoa-Tapia, Natural convection in a cylindrical porous cavity with internal heat source: a numerical study with Brinkman-extended Darcy model, Int. J. Heat Mass Transfer 42 (1999) 4185–4195.

[3] F. Stroh, V. Balakotaiah, Stability of uniform flow in packed-bed reactors, Chem. Eng. Sci. 47 (1992) 593–604.

[4] D. Nguyen, V. Balakotaiah, Flow maldistributions and hot spots in down-flow packed bed reactors, Chem. Eng. Sci. 49 (1994) 5489–5505.

[5] V. Yakhnin, M. Menzinger, Stationary and traveling hot spots in the catalytic combustion of hydrogen in monoliths, Chem. Eng. Sci. 57 (2002) 4559–4567.

[6] F.P. Incropera, Convection heat transfer in electronic equipment cooling, ASME J. Heat Transfer 110 (1988) 1097–1111.

[7] M.S. Polentini, S. Ramadhyani, F.P. Incropera, Single-phase thermosyphon cooling of an array of discrete heat sources in a rectangular cavity, Int. J. Heat Mass Transfer 6 (1993) 939–954.

[8] L. Tang, K.A. Moores, C. Ramaswamy, Y. Joshi, Characterizing the thermal performance of a flow through electronics module using a porous media model, in: Proceedings of the 14th IEEE Semi-Thermal Symposium, 1998, pp. 68–77.

[9] T. Heindel, F.P. Incropera, S. Ramadhyani, Enhancement of natural convection heat transfer from an array of discrete heat sources, Int. J. Heat Mass Transfer 39 (1996) 479–490.

[10] V. Prasad, F.A. Kulacki, M. Keyhani, Natural convection in porous media, J. Fluid Mech. 150 (1985) 89–119.

[11] C.-K. Chen, C.-H. Chen, W.J. Minkowycz, U.S. Gill, Non-Darcian effects on mixed convection about a vertical cylinder embedded in a saturated porous medium, Int. J. Heat Mass Transfer 35 (1992) 3041–3046.

[12] W.J. Minkowycz, A. Haji-Sheikh, K. Vafai, On departure from local thermal equilibrium in porous media due to rapidly changing heat source: the Sparrow number, Int. J. Heat Mass Transfer 42 (1999) 3373–3385.

[13] S.M. Alex, P.R. Patil, K.S. Venkatakrishnan, Variable gravity effects on thermal instability in a porous medium with internal heat source and inclined temperature gradient, Fluid Dyn. Res. 29 (2001) 1–6.

[14] M.C. Kim, S.B. Lee, B.-J. Chung, S. Kim, Heat transfer correlation in fluid-saturated porous layer under uniform volumetric heat sources, Int. Commun. Heat Mass Transfer 29 (2002) 1089–1097.

[15] A. Amiri, K. Vafai, Analysis of dispersion effects and non-thermal equilibrium, non-Darcian, variable porosity incompressible flow through porous media, Int. J. Heat Mass Transfer 37 (1994) 939–954.

[16] J.A. Deiber, R.A. Bortolozzi, A two-field model for natural convection in a porous annulus at high Rayleigh numbers, Chem. Eng. Sci. 53 (1998) 1505–1516.

[17] G. Lauriat, V. Prasad, Non-Darcian effects on natural convection in a vertical porous enclosure, Int. J. Heat Mass Transfer 32 (1989) 2135–2148.

[18] A. Amiri, K. Vafai, Transient analysis of incompressible flow through a packed bed, Int. J. Heat Mass Transfer 41 (1998) 4259–4279.

[19] D.-Y. Lee, K. Vafai, Analytical characterization and conceptual assessment of solid and fluid temperature differentials in porous media, Int. J. Heat Mass Transfer 42 (1999) 423–435.

[20] R.A. Bortolozzi, J.A. Deiber, Comparison between two- and one-field models for natural convection in porous media, Chem. Eng. Sci. 56 (2001) 157–172.

[21] K. Vafai, Convective flow and heat transfer in variable-porosity media, J. Fluid Mech. 147 (1984) 233–259.

[22] D. Kunii, J. Smith, Heat transfer characteristics of porous rocks, AIChE J. 6 (1960) 71–78.

[23] N. Wakao, S. Kaguei, T. Funazkri, Effect of fluid dispersion coefficients on particle-to-fluid heat transfer coefficients in packed beds, Chem. Eng. Sci. 34 (1979) 325–336.

[24] A.G. Dixon, D.L. Cresswell, Theoretical prediction of effective heat transfer parameters in packed beds, AIChE J. 25 (1979) 663–676.

[25] J.W. Mercer, C.R. Faust, W.J. Miller, F.J. Pearson, Review of simulation techniques for aquifer thermal energy storage, Adv. in Hydrosci. 13 (1982) 1–129.

[26] P. Cheng, C.T. Hsu, Applications of Van Driest's mixing theory to transverse thermal dispersion in forced convective flow through a packed bed, Int. Commun. Heat Mass Transfer 13 (1986) 613–625.

[27] F.C. Lai, V. Prasad, F.A. Kulacki, Aiding and opposing mixed convection in a vertical porous layer with a finite wall heat source, Int. J. Heat Mass Transfer 31 (1988) 1049–1061.

[28] J.G. Georgiadis, I. Catton, Free convective motion in an infinite vertical porous slot: the non-Darcian regime, Int. J. Heat Mass Transfer 28 (1985) 2389–2392.

[29] V. Prasad, F.A. Kulacki, Convective heat transfer in a rectangular porous cavity. Effect of aspect ratio on flow structure and heat transfer, ASME J. Heat Transfer 106 (1984) 158–165.

[30] J.G. Georgiadis, I. Catton, Dispersion in cellular thermal convection in porous layers, Int. J. Heat Mass Transfer 31 (1988) 1081–1091.

[31] G.Z. Gershuni, D.V. Lyubimov, in: Thermal Vibrational Convection, J. Wiley and Sons, New York, 1998, p. 148.